Research Article | Vol. 27, No. 7 | 1 Apr 2019 | OPTICS EXPRESS 9655

Optics EXPRESS

Single-ring suspended fiber for Bragg grating based hydrostatic pressure sensing

LIN HTEIN, ZHENGYONG LIU,* DINUSHA GUNAWARDENA, AND HWA-YAW TAM

Photonics Research Centre, Department of Electrical Engineering, The Hong Kong Polytechnic University, Hung Hom, Kowloon, Hong Kong SAR
**zhengyong.liu@connect.polyu.hk*

Abstract: We present a novel optical fiber composed of a suspended core, a supporting ring and an outer ring. To establish a large holey region, a germanium-doped core is suspended by a silica ring and the entire structure is enclosed by another silica ring. By monitoring the Bragg wavelength shift of an FBG written in such a fiber with an air filling fraction of 65%, a hydrostatic pressure sensitivity of –43.6 pm/MPa was achieved experimentally. The high-pressure sensitivity is in good agreement with the numerically calculated value of ~40 pm/MPa. Due to the significant impact of the fiber core suspended in the large holey region inside the fiber, the pressure sensitivity improved by approximately eleven times compared to a Bragg grating inscribed in a standard single-mode fiber. To the best of our knowledge, it is the highest pressure sensitivity obtained for a FBG-based sensor experimentally, when compared to other FBG-based pressure sensors reported up to date. The large air hole region and the suspended core in the center of the fiber not only make the proposed fiber sensor a good candidate for pressure measurements, especially in the oil industry where space is at a premium, but also allow the detection of substances, by exploiting interaction of light with liquids or gases.

1. Introduction

Microstructured optical fibers (MOF) provide an excellent platform for fiber sensors due to their flexibility in design and fabrication. MOFs are used in monitoring physical and biochemical parameters such as strain, temperature, pressure, curvature, vibration, torsion, humidity, refractive index, chemicals and gases [1,2]. A number of MOFs have been developed through modification of their internal structures [3]. However, since most MOFs are constructed with a fiber core surrounded by one or more layers of air-holes in the cladding, the research focus usually revolves on the arrangement of air-holes in the MOFs to achieve high sensitivity or birefringence [4,5].

It has been suggested that pressure sensitivity can be improved by increasing the size of the air-holes [6] or by placing the air-holes in close proximity to the core of the fiber [4]. Thereby, nearly six-times enhanced sensitivities have been previously reported in two-hole fibers having a pair of 15-μm and 90-μm air-holes [7,8], and side-hole fibers [9]. In a study of MOFs with the core supported by three strands [10], the concept of reducing the outer-wall thickness or strand thickness has been proposed to enhance the sensitivity. Generally, air-filling fraction (AFF), the ratio of air region to total cross-sectional area in the structure, is enlarged by reducing the number of air-holes around the core to make the cross-sectional region of silica smaller. Relating to the size of air-holes, a pressure sensor based on a large-hole grapefruit MOF [11] has already shown good performance. By minimizing the number of air-holes to two, the pressure response in a side-hole fiber has managed to yield a 200 times improvement compared to that achieved by an elliptical-core fiber [12]. Two large side-holes along the length of the MOF's cladding induce an anisotropic stress in the core region, resulting in a high polarimetric sensitivity to pressure that reached a sensitivity of −100 nm/MPa [13]. Depending on the detected pressure range, pressure sensitivity of a Sagnac

#355827 https://doi.org/10.1364/OE.27.009655
Journal © 2019 Received 20 Dec 2018; revised 1 Mar 2019; accepted 4 Mar 2019; published 20 Mar 2019

Optics EXPRESS

interferometer constructed based on a two-semicircle holes MOF reaches the value of 50 nm/MPa [14].

Although interferometric techniques show high pressure sensitivities, generally, these types of sensing principles impose a limitation on the length of the sensor head [15]. The interferometric technique associated with birefringent fibers requires a long sensing fiber to determine pressure-induced phase change since shortening the length of the sensing fiber results in a broad wavelength spacing between the transmission peaks, which lowers the detecting accuracy. In addition, the techniques normally require a highly coherent light source as well as a coupler to detect pressure variation, and it can be challenging to multiplex more sensors in a single strand of fiber. On the other hand, fiber Bragg gratings (FBGs) based sensors are capable of being multiplexed and compact; measurements are highly repeatable and more reliable compared to other sensing schemes. Nevertheless, FBGs fabricated in conventional single-mode fibers (SMFs) have low pressure sensitivities of 3-4 pm/MPa [16] compared to other measurands [17,18]. Although, Bragg gratings written in grapefruit MOFs and two-hole fibers [11,19] exhibit an improved sensitivity compared to that of SMF, the pressure sensitivity remains at a value lower than –13 pm/MPa. However, through effective modification of the structure of the MOF, the pressure sensitivity can be enhanced.

In this paper, we have proposed and experimentally demonstrated a novel design which contains a central core, referred to as a suspended core, supported by a single silica ring. Besides maintaining the suspended core in the center of the structure, the ring also introduces a large holey region and a geometrical asymmetry. Owing to the significant increase in the AFF, external pressure induces a large wavelength shift in the FBG that cannot be achieved in conventional SMFs [16] or other types of MOFs [11,19]. To the best of our knowledge, the sensitivity of –43.6 pm/MPa achieved in this experiment using the proposed single-ring suspended fiber is the highest value reported in a FBG-based pressure sensor. Consequently, we have performed a numerical simulation enabling to optimize the best possible pressure sensitivity. It has been verified that the larger the AFF in this particular fiber, the more sensitive it is to pressure. Single-ring suspended fibers with two different AFFs have been explored in this study and an improvement in pressure sensitivity by a factor of two has been observed when the AFF was raised from 44% to 65%. This observation has been experimentally demonstrated as well. In addition, the proposed sensor based on a single-ring suspended fiber offers good stability, low temperature cross-sensitivity and easy splicing with SMFs permitting multiple sensors to be multiplexed along a single optical fiber.

2. Principle of operation

For FBG-based fiber sensors, the Bragg wavelength, which is a function of the effective refractive index of the fundamental mode (n_{eff}) and the grating pitch (Λ), is determined by the expression:

$$\lambda_B = 2n_{eff}\Lambda. \tag{1}$$

When a FBG is under hydrostatic pressure, both n_{eff} and Λ will change corresponding to the pressure, which can be expressed by:

$$\lambda'_B = 2n'_{eff}\Lambda' = 2(n_{eff} + \Delta n_{eff})(\Lambda + \Delta\Lambda) \approx \lambda_B\left(1 + \frac{\Delta n_{eff}}{n_{eff}} + \frac{\Delta\Lambda}{\Lambda}\right), \tag{2}$$

where, n'_{eff} is the effective refractive index of the fundamental mode and Λ' is the grating period after applying pressure, $\Delta n_{eff} = n'_{eff} - n_{eff}$ is the pressure-induced change in effective refractive index and $\Delta\Lambda = \Lambda' - \Lambda$ is the pressure-induced change in the grating period. Therefore, the Bragg wavelength shift can be formulated as:

$$\frac{\Delta\lambda_B}{\lambda_B} = \frac{\Delta n_{eff}}{n_{eff}} + \frac{\Delta\Lambda}{\Lambda} = \frac{\Delta n_{eff}}{n_{eff}} + \varepsilon_{z,pressure}. \quad (3)$$

As clearly seen from Eq. (3), to improve the pressure sensitivity of a FBG-based sensor, two approaches can be employed. One such approach is to introduce a large change in the effective refractive index in the presence of a constant pressure, where more stress is transferred to the core of the optical fiber based on the photo-elastic effect. The second approach is to reduce the rigidity of the fiber to enlarge the axial strain. Both these approaches can be achieved easily by introducing air holes in the fiber, especially to reduce the rigidity, thereby, reducing Young's modulus. The equivalent Young's modulus of the microstructured optical fiber can be [20]

$$E' = (1-\eta)E, \quad (4)$$

where, E is the Young's modulus of the silica glass, which is 73.1 GPa; E' is the equivalent Young's modulus. The Poisson ratio of the effective solid model of the MOF is regarded as same as that of silica glass, which is 0.17; η is the AFF.

3. Fiber fabrication and characterization

The pressure sensitivity of a FBG-based pressure sensor can be enhanced by increasing the AFF, which leads to a larger axial strain (ε_z) due to less stiffness in the material. Based on this aspect, a single-ring suspended fiber is proposed in this study which shows a high AFF and a low refractive index change. Two types of such fibers were designed and fabricated. The scanning electronic microscopic (SEM) images of the cross-sections of these fibers are shown in Fig. 1.

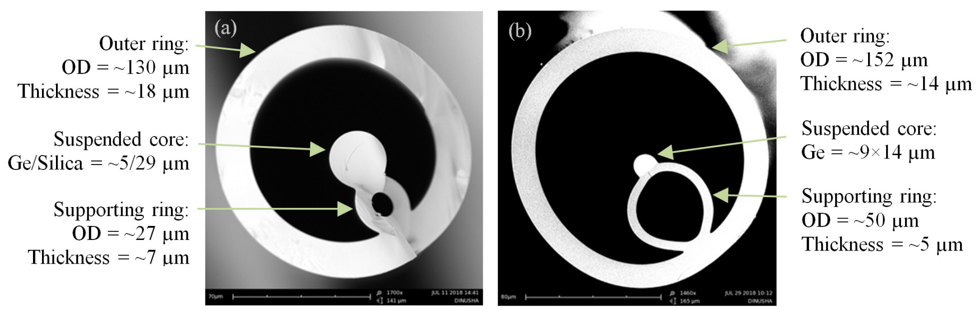

Fig. 1. SEM images of the single-ring suspended fibers: (a) Fiber-1 and (b) Fiber-2.

The fibers were fabricated using the stack-and-draw technique. Two different wall thicknesses and core sizes were chosen to prepare the preforms, which were eventually drawn to two types of fibers, referred to as Fiber-1 and Fiber-2, with small and large AFFs, respectively. In the preparation of the Fiber-1 preform, an outer tube consisting of an inner/outer diameter (ID/OD) of 19/25-mm was used. A germanium (Ge)-doped rod with a core and cladding diameter of 1-mm and 5.4-mm was incorporated at the center of the stacked tube. To introduce a large air region inside the fiber, the Ge-doped rod was suspended using a supporting tube with an ID/OD of 4/6.2-mm. Five supplementary tubes, which are of the same size as the supporting tube but shorter in length, were stacked together at the end of the preform to hold the structure in place and to center the core rod. Following the same stacking procedure, Fiber-2 preform was then prepared mainly by reducing the thicknesses of the tubes to further increase the AFF. The tubes ought to be prepared as thin as possible to maximize the sensitivity of the sensor. However, if the wall thickness of the preform is too thin, it complicates the process of maintaining the shape of the fiber at high drawing temperatures which can cause serious deformations in the fiber structure. The ID/OD of the outer tube and

Optics EXPRESS

the supporting tube used during stacking of the Fiber-2 preform were 14/16 mm and 5.9/6.6 mm, respectively, and the diameter of the Ge-doped core rod was 1 mm. Without applying any pressure, the two fibers were drawn at ~1920 °C, which is relatively low compared to the drawing temperature of a solid fiber which aids in maintaining the structure. Fiber drawing tension was kept under 0.7 N. Such a low drawing temperature with low tension is a constraint in the fabrication process. When drawing a single-ring suspended fiber with an optimum geometry, various parameters in the fiber drawing process need to be adjusted depending on the thickness of the tubes and the size of the preform. This allows the experiment to be successfully reproduced using the optimized drawing conditions.

As shown in Fig. 1, in Fiber-1, the Ge-doped core is surrounded by silica with a thickness of 12-µm whereas the suspended core of Fiber-2 is fully doped with Ge. The difference in the refractive indices between the core and cladding of Fiber-1 and Fiber-2 are 0.42% and 0.62%, respectively. Fiber-1 has an outer diameter of 130-µm and a polyimide coating with a thickness of 10 µm whereas Fiber-2 has an outer diameter of ~150-µm and an acrylate coating with a thickness of 30-µm. Fiber parameters such as the core and cladding diameters, the ring thicknesses and AFFs are listed in Table 1.

Attenuations of the fibers were measured by the standard cutback method, and were estimated to be 0.06 dB/m and 16 dB/m at 1550 nm for Fiber-1 and Fiber-2, respectively. The orientation of the fiber needs to be adjusted while cleaving the fiber end in such a way so that the end face is in the appropriate condition when the supporting ring is opposite to the blade of the optical fiber cleaver (Fitel S323). The fibers can be easily spliced to SMF with average splice losses of 1.0 dB/splice and 2.9 dB/splice for Fiber-1 and Fiber-2, respectively. The existence of thinner walls and the absence of a silica cladding around the suspended core resulted in a higher attenuation and splice loss of Fiber-2 compared to those of Fiber-1.

4. Pressure measurement and analysis

4.1 Theoretical calculation results

With reference to Fig. 1, when pressure is applied to the outer boundary of the fiber, the induced stress is transferred to the core region, which eventually changes the refractive index owing to the photo-elastic effect. The relationship can be expressed as [14]

$$\begin{bmatrix} \Delta n_x \\ \Delta n_y \\ \Delta n_z \end{bmatrix} = \begin{bmatrix} C_1 & C_2 & C_2 \\ C_2 & C_1 & C_2 \\ C_2 & C_2 & C_1 \end{bmatrix} \begin{bmatrix} \sigma_1 \\ \sigma_2 \\ \sigma_3 \end{bmatrix}, \tag{5}$$

where, Δn_i ($i = x, y, z$) is the refractive index change in the fiber, σ_i ($i = 1, 2, 3$) is the principle component of the pressure-induced stress; C_1, C_2 are the stress-optic coefficients and are -0.65×10^{-12} m^2/N and -4.2×10^{-12} m^2/N, respectively [21]. Using the finite element method (FEM) stress analysis in COMSOL Multiphysics, the effective index of the fundamental mode and the stress distribution under various pressures can be calculated. Figures 2(a) and 2(c) show the simulated mode profiles; Figs. 2(b) and 2(d) are the stress distributions of Fiber-1 and Fiber-2, respectively. It can be clearly seen that both fibers support propagation of the fundamental mode and there is a minimum transfer of pressure-induced stress to the core region, which eventually results in a small index change. Figures 2(e) and 2(f) indicate the effective refractive index change ratio ($\Delta n_{eff}/n_{eff}$) with respect to the applied pressure for Fiber-1 and Fiber-2, respectively. According to the results obtained, the effective refractive index change ratio is considerably small, in the order of 10^{-7}-10^{-6}. Particularly for Fiber-1, the AFF is altered by changing the thickness of the outer tube to 150 µm, 130 µm, and 110 µm, which resulted in AFFs of 0.33, 0.44 and 0.62, respectively. The effective refractive index change ratio gradually increases with the reduction of the thickness. On the other hand, the outer diameter of Fiber-2 is scaled down from 152 µm to 125 µm and subsequently to 100 µm

Optics EXPRESS

while maintaining the AFF at 0.65. It is observed from the results in Fig. 2(f) that the effective refractive index change ratio slightly increases with the reduction of the tube thickness but remains at a level of ~10^{-6}. The reason responsible for this effect is the special structure of this fiber, in which the core is almost separated from the cladding tube and therefore, is minimally affected by the ambient pressure. Since the refractive index change ratio is positive whereas the axial strain is negative (as analyzed below), a smaller variation in the refractive index change ratio is desirable to enhance the pressure sensitivity, as shown in Eq. (3).

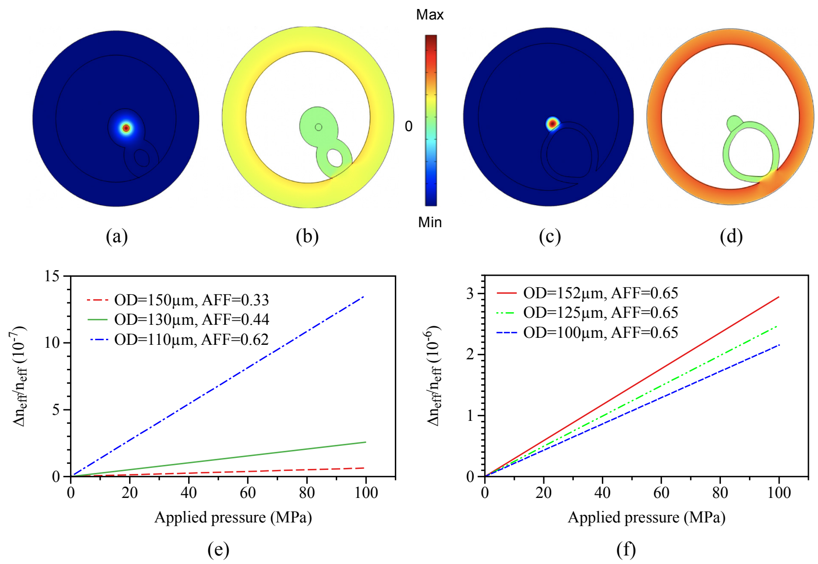

Fig. 2. Simulation results of the single-ring suspended fiber. (a) The simulated mode profile and (b) stress distribution (P = 100MPa) of Fiber-1; (c) simulated mode profile and (d) stress distribution (P = 100MPa) of Fiber-2; effective index change ratio for different AFFs as a function of applied pressure in (e) Fiber-1 and (f) Fiber-2.

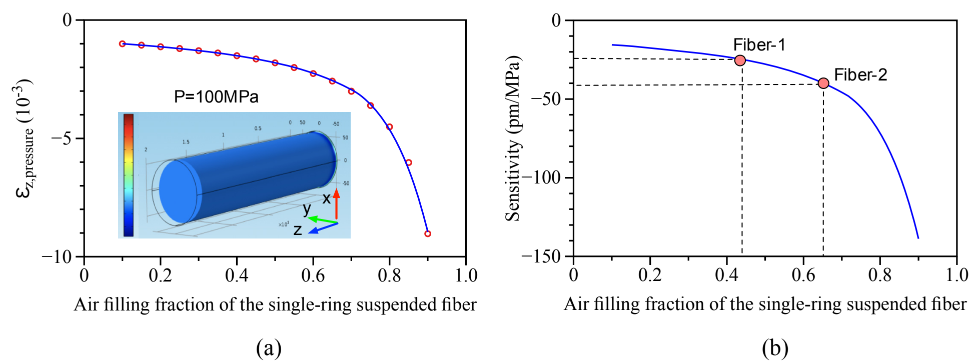

Fig. 3. (a) Calculated axial strain ($\varepsilon_{z,\ pressure}$) induced by a pressure of 100 MPa using the effective solid fiber based on the equivalent Young's modulus under different AFFs; (b) calculated pressure sensitivity as a function of AFF.

When the fiber is subjected to ambient pressure, the induced axial strain, affects the pitch of the FBG written in the fiber. Figure 3(a) shows the axial strain induced by a pressure of 100 MPa with respect to different AFFs based on the model of an effective solid fiber in accordance with the equivalent Young's modulus as shown in Eq. (4). It is noticed that the pressure-induced axial strain is negative and in the order of 10^{-3}, which means that the axial strain dominates the Bragg wavelength shift of such a fiber. A higher AFF leads to a larger

Optics EXPRESS

axial strain and higher sensitivity. Figure 3(b) shows the calculated pressure sensitivity of the single-ring suspended fiber without considering the effect of the refractive index change ratio. The sensitivity can be improved by increasing the AFF, e.g. reducing the thickness of the cladding tube, supporting tube and the silica region close to the core, which is the case in Fiber-2. At 1550 nm, the calculated sensitivity for Fiber-1 (AFF = 0.44) and Fiber-2 (AFF = 0.65) are –25.4 pm/MPa, and –40 pm/MPa, respectively. In comparison, the same approach was employed to calculate the sensitivity of SMF (i.e. AFF = 0), which is –4.6 pm/MPa, much lower than the proposed fiber with a larger AFF. The negative value indicates a blue shift in the Bragg wavelength with increasing pressure.

4.2 Experiment

Prior to the FBG inscription process, the two fibers were loaded in a hydrogen chamber for a week at a pressure of 120-bars and the FBGs were written with the aid of a 248-nm laser and a phase mask. The reflection spectra of the FBGs in Fiber-1 and Fiber-2 under zero pressure are presented in Fig. 4(a). The grating lengths are 10 mm and the Bragg wavelengths of FBGs are 1545.465 nm and 1545.075 nm for Fiber-1 and Fiber-2, respectively. Higher-order modes exist due to the large refractive index contrast between the core and air region resulting in several resonance peaks in the FBG spectrum profiles.

Figure 4(b) shows the schematic diagram of the hydrostatic pressure sensing experiment. To perform the pressure test, one end of a segment of the single-ring suspended fiber comprising of the FBG was spliced with SMF whereas the other end of the single-ring suspended fiber was completely sealed to avoid any inflow of hydraulic oil into the holey region. However, if necessary, based on the relevant application, it is also possible for more sensors to be multiplexed. The pressure chamber used in this experiment is 900-mm long and has an inner diameter of 22-mm. Pressure inside the chamber was increased gradually from 0 to 52 MPa in steps of 4 MPa. The applied pressure was calibrated using a pressure gauge (CONST 211) and the shift in the Bragg wavelength was monitored using an interrogator (Micron Optics SM125) with an accuracy of 1 pm. Fiber-1 and Fiber-2 were tested to study the influence of AFF on the pressure sensitivity. The tests were repeated three times to evaluate the repeatability of the sensor. Similarly, a conventional SMF was also tested under the same pressure loading conditions to characterize the pressure response of the proposed sensor.

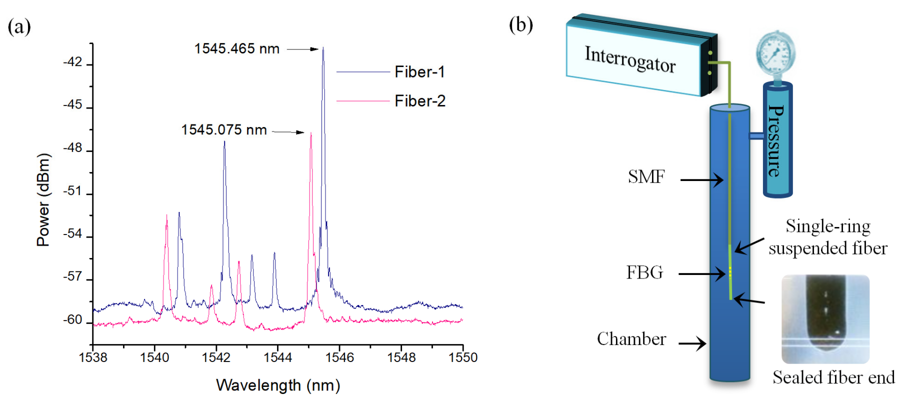

Fig. 4. (a) Reflected spectra of the FBGs inscribed in single-ring suspended fibers; (b) configuration of the experimental setup used to measure pressure-induced Bragg wavelength shifts.

5. Results and discussion

By applying hydrostatic pressures in the range of 0 to 52 MPa to the sensor, Bragg wavelength shifts of the single-ring suspended fibers were recorded and the obtained results

Optics EXPRESS

are demonstrated in Fig. 5(a). During the experiment, the Bragg wavelength blue shifts with increasing hydrostatic pressure. The negative strain implies that the contribution of the axial strain is larger than that of the radial strain induced by the pressure [11]. Experimentally measured sensitivities of Fiber-1 and Fiber-2 to hydrostatic pressure were –22.2 pm/MPa and –43.6 pm/MPa, respectively, whereas that of SMF amounted to –3.9 pm/MPa. In comparison with SMF, the pressure sensitivities of Fiber-1 and Fiber-2 were about 6 times and 11 times higher, indicating a large improvement in the presence of a large air hole region. The enhancement in the pressure sensitivity of Fiber-2 which was about two times is attributed to the increase of AFF from 44% to 65%. Moreover, an experimental investigation on the effect of the length of the sensing fiber on the pressure response was carried out and the results obtained are shown in Fig. 5(b). It was observed that there is insignificant effect on the pressure response of the FBG with respect to the length of the sensing fiber. In Fiber-2 with lengths of 16-mm and 85-mm, pressure sensitivities of –43.6 pm/MPa and –42.1 pm/MPa, respectively were obtained. Pressure tests were repeated three times for each fiber and the mean values of the data with error bars are shown in Fig. 5. The straight lines are the linear fits of the data. A linear relationship between the hydrostatic pressure and the Bragg wavelength shift is observed with a R^2 value in the range of 0.99908 to 0.99991 in the tests of all the single-ring suspended fibers. The parameters and sensitivities of the sensors are compared in Table 1. The analytical results of –4.6 pm/MPa, –25.4 pm/MPa and –40.0 pm/MPa for SMF, Fiber-1 and Fiber-2, respectively, are consistent with the experimental values. The small discrepancy between the calculated and measured values is possibly due to the slight deformation in the structure under the actual pressure.

Table 1. Comparison of Fiber Parameters and Their Respective Pressure Responses

Fiber	*Core diameter (µm)*	*Cladding diameter (µm)*	*Outer-ring thickness (µm)*	*Supporting-ring diameter (µm)*	*Supporting-ring thickness (µm)*	*AFF (%)*	*Theoretical sensitivity (pm/MPa)*	*Experimental sensitivity (pm/MPa)*
SMF	8.0	125	-		-	0	–4.6	–3.9
Fiber-1	5.0	130	18	27	7	44	–25.4	–22.2
Fiber-2	9 × 14	152	14	50	5	65	–40.0	–43.6

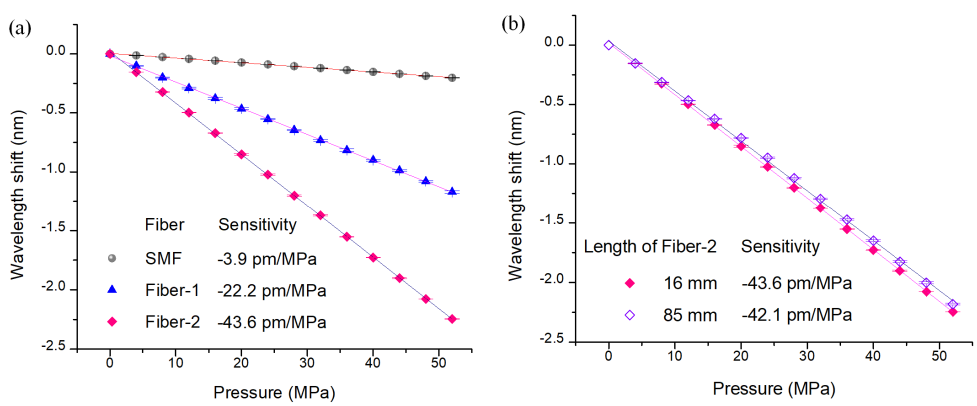

Fig. 5. (a) Pressure responses of SMF and single-ring suspended fibers: Fiber-1 and Fiber-2; (b) pressure responses of Fiber-2 measured at two different fiber lengths.

In addition, temperature variation of the sensor is also considered in practical applications as the FBG is exposed to temperature perturbations. Shifts in the Bragg wavelengths of Fiber-1 and Fiber-2 due to change in temperature are illustrated in Fig. 6. Straight lines indicate the linear fit curves corresponding to the wavelength shifts at different applied temperatures. Linear fits of the obtained data indicate temperature responses of 11.5 pm/°C and 10.8 pm/°C for Fiber-1 and Fiber-2, respectively and therefore, the temperature cross-sensitivities can be calculated as 0.52 MPa/°C and 0.25 MPa/°C, respectively. Despite the fact that the temperature responses of proposed sensors are similar to that of SMF [16], the temperature cross-sensitivity of the single-ring suspended fiber is much lower compared to that of SMF (3.44 MPa/°C).

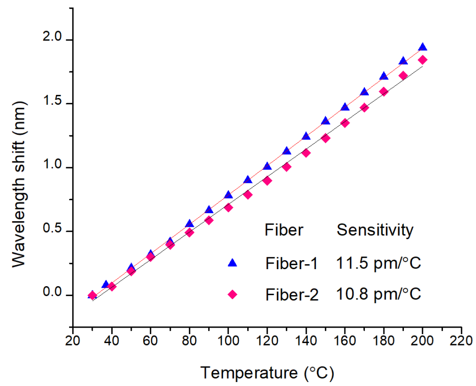

Fig. 6. Temperature responses of single-ring suspended fibers: Fiber-1 and Fiber-2.

Table 2 summarizes reported techniques used in measuring the wavelength shift depending on the variation in pressure. The techniques are based on FBGs where measurements are carried out either by detecting the peak shifts or peak separations in Bragg wavelengths using various kinds of specialty optical fibers. Other than SMF, MOFs are often used to construct pressure sensors since their structures offer unique opportunities in tailoring the optical and mechanical effects. Compared to SMF [16], the pressure sensitivity of the proposed sensor is improved by over 14 times, which is, to our knowledge, the highest value reported for a hydrostatic pressure sensor based on grating technique. Compared to FBGs in grapefruit MOFs [11] and two-hole fibers [19], the pressure sensitivity obtained in this work is enhanced by 3.4 times and is 1.6 times larger to that of a FBG in a glass-bubble housing [22]. In the glass-bubble housing technique, mechanical compliance of a hollow glass bubble which acts as an amplifier is greater than that of a solid fiber; hence, the pressure sensitivity is enhanced relative to a bare SMF. Monitoring the wavelength separation of Bragg peaks related to the change in pressure-induced birefringence, experimental hydrostatic pressure sensitivities of −15 pm/MPa and 33 pm/MPa have been reported in highly birefringent MOFs [5]. Owing to the peak separation based strategy, the sensor is insensitive to temperature perturbations. However, small deformation of the microstructures in such fibers and repeatability of the fiber are hard to control. Furthermore, even small differences in the drawing conditions may result in different birefringence and sensitivities.

Table 2. Comparison of Several Hydrostatic-Pressure Sensing Techniques Specifically Based on FBGs

No.	Technique	Fiber	Sensitivity (pm/MPa)	Ref.
1	FBG	SMF	–3.04	[16]
2	FBG	Grapefruit MOF	–12.86	[11]
3	FBG peak separation	Two-hole fiber	–12.89	[19]
4	FBG in a glass-bubble housing	SMF	–27.77	[22]
5	FBG peak separation	Birefringence MOF	–15 (MOF1), 33 (MOF2)	[5]
6	FBG	Single-ring suspended fiber	– 43.6	This work

Generally, FBG based techniques are much less sensitive to pressure than the interferometric techniques [13,14,23]. The interferometric sensors also have detection limits which are determined by the Q factor of the sensors and the detecting accuracy of the spectral shifts [24]. Besides, other techniques usually require either a highly coherent light source or

Optics EXPRESS

non-fiber components (e.g. coupler, polarizer) combined with sophisticated readout schemes. The operating pressure range is sometimes limited by the pressure-induced phase difference between two orthogonal-polarization modes. In our experiment, the maximum hydrostatic pressure applied to the sensor is limited by the experimental setup used. Nevertheless, it is expected to have a much higher pressure range.

The fabrication and packaging of FBG sensors are relatively simpler compared to other sensing schemes, due to their small dimensions and considerable low cost. The proposed technique based on FBGs has high pressure sensitivity and repeatability. Based on the bandwidth of the FBG (3-dB bandwidth is ~0.07-nm, in this work), the sensitivity can be calibrated more accurately with the length of the sensor being only a few millimeters whereas it is challenging for interferometric techniques to achieve a similar performance in such short lengths. In the proposed fiber structure, Fiber-1 shows low sensitivity to bending because apart from helping to reduce the splicing loss and attenuation, the silica around the core also assists to confine the light inside the core [25]. Bending losses of Fiber-1 and Fiber-2 at 1550 nm were measured to be about 0.016 dB/turn and 0.17 dB/turn, respectively with a coiling diameter of 10-mm. Both are small enough owing to the suspended strucutre.

Although the propagation loss of Fiber-2 is higher than Fiber-1, it remains within an acceptable range for most applications since FBG based sensing systems do not need long lengths of fiber. The cause of higher loss in Fiber-2 compared to Fiber-1, is due to the pure Ge-doped core without a silica cladding. However, this cannot affect the high sensitivity of the sensor because the variation of the grating peak power is only ~0.3 dB for a 16 mm-long fiber. On the other hand, attenuation of the fiber can easily be reduced by incorporating a thin silica cladding around the core with a core/cladding ratio of 80-90% instead of using a pure Ge-core rod to achieve a similar performance.

6. Conclusion

We have presented two kinds of single-ring suspended fibers in which the cores are suspended by a single silica ring and the entire structure enclosed by an annular ring. These two fibers possess a holey region with air-filled fractions (AFFs) of 44% (Fiber-1) and 65% (Fiber-2), and propagation losses of ~0.06 dB/m and ~16 dB/m, respectively. Pressure sensing characteristics of Bragg gratings inscribed in these specially designed fibers were investigated numerically and experimentally. For this particular fiber structure, the simulation results have shown that the pressure sensitivity can be improved significantly by enlarging the AFF. The calculated pressure sensitivities for Fiber-1 and Fiber-2 are –25.4 pm/MPa and –40.0 pm/MPa, respectively. To confirm the high-pressure sensitivity, the pressure measurements were conducted using the FBGs written in the fabricated fibers and sensitivities of –22.2 pm/MPa and –43.6 pm/MPa were obtained for Fiber-1 and Fiber-2, respectively whereas that of single-mode fiber (SMF) was measured to be only –3.9 pm/MPa. Owing to the novel structure, the pressure sensitivity has enhanced approximately to eleven times compared to SMF, and also higher than those obtained by FBGs written in all the other MOFs. A detailed comparison of pressure sensors reported using the grating technique was conducted in an effort to demonstrate the competitive performance of the proposed sensor. Owing to the advantages of compactness, capability of multiplexing sensors, high detection accuracy and high sensitivity, the proposed FBG-based pressure sensor is ideal for a wide range of applications requiring high pressure measurements including oil industries. Due to isolation of the fiber core from the surrounding medium, the fiber can be embedded in various types of materials such as concrete, gypsum, etc. avoiding any spectral distortion in the spectrum profile of the grating. Moreover, the large air hole region and the small suspended core in the center of the fiber allow interaction between light and any other additional substance (e.g. liquid, gas), making it a good candidate for other types of applications as well.

Optics EXPRESS

Funding

Hong Kong Polytechnic University (1-ZVGB, 1-BBYE, 1-BBYS).

References

1. A. M. Pinto and M. Lopez-Amo, "Photonic crystal fibers for sensing applications," J. Sens. **2012**, 1–21 (2012).
2. T. G. Euser, J. Chen, M. Scharrer, P. S. J. Russell, N. J. Farrer, and P. Sadler, "Quantitative broadband chemical sensing in air-suspended solid-core fibers," J. Appl. Phys. **103**(10), 103108 (2008).
3. P. Kaiser and H. Astle, "Low-loss single-material fibers made from pure fused silica," Bell Syst. Tech. J. **53**(6), 1021–1039 (1974).
4. C. M. Jewart, S. M. Quintero, A. M. B. Braga, and K. P. Chen, "Design of a highly-birefringent microstructured photonic crystal fiber for pressure monitoring," Opt. Express **18**(25), 25657–25664 (2010).
5. S. Sulejmani, C. Sonnenfeld, T. Geernaert, P. Mergo, M. Makara, K. Poturaj, K. Skorupski, T. Martynkien, G. Statkiewicz-Barabach, J. Olszewski, W. Urbanczyk, C. Caucheteur, K. Chah, P. Megret, H. Terryn, J. Van Roosbroeck, F. Berghmans, and H. Thienpont, "Control over the pressure sensitivity of Bragg grating-based sensors in highly birefringent microstructured optical fibers," IEEE Photonics Technol. Lett. **24**(6), 527–529 (2012).
6. M. Liao, C. Chaudhari, X. Yan, G. Qin, C. Kito, T. Suzuki, and Y. Ohishi, "A suspended core nanofiber with unprecedented large diameter ratio of holey region to core," Opt. Express **18**(9), 9088–9097 (2010).
7. S. Kreger, S. Calvert, and E. Udd, "High pressure sensing using fiber Bragg gratings written in birefringent side hole fiber," in *15th Optical Fiber Sensors Conference Technical Digest* (2002), pp. 355–358.
8. C. Jewart, D. Xu, K. P. Chen, and J. Canning, "Structure optimization of air-hole fibers for high-sensitivity fiber Bragg grating pressure sensors," in *19th International Conference on Optical Fibre Sensors* (International Society for Optics and Photonics 2008).
9. S. S. J. R. Clowes and M. N. Zervas, "Pressure sensitivity of side-hole optical fiber sensors," IEEE Photonics Technol. Lett. **10**,(6) 857859 (1995).
10. W. N. MacPherson, E. J. Rigg, J. D. Jones, V. Kumar, J. C. Knight, and P. S. J. Russell, "Finite-element analysis and experimental results for a microstructured fiber with enhanced hydrostatic pressure sensitivity," J. Lightwave Technol. **23**(3), 1227–1231 (2005).
11. C. Wu, B.-O. Guan, Z. Wang, and X. Feng, "Characterization of pressure response of Bragg gratings in grapefruit microstructured fibers," J. Lightwave Technol. **28**(9), 1392–1397 (2010).
12. R. Kaul, "Pressure sensitivity of rocking filters fabricated in an elliptical-core optical fiber," Opt. Lett. **20**(9), 1000–1001 (1995).
13. J. A. Croucher, L. Gomez-Rojas, S. Kanellopoulos, and V. A. Handerek, "Approach to highly sensitive pressure measurements using side-hole fibre," Electron. Lett. **34**(2), 208–209 (1998).
14. Z. Liu, L. Htein, K.-K. Lee, K.-T. Lau, and H.-Y. Tam, "Large dynamic range pressure sensor based on two semicircle-holes microstructured fiber," Sci. Rep. **8**(1), 65 (2018).
15. H. Y. Fu, C. Wu, M. L. V. Tse, L. Zhang, K.-C. D. Cheng, H. Y. Tam, B.-O. Guan, and C. Lu, "High pressure sensor based on photonic crystal fiber for downhole application," Appl. Opt. **49**(14), 2639–2643 (2010).
16. M. Xu, L. Reekie, Y. Chow, and J. P. Dakin, "Optical in-fibre grating high pressure sensor," Electron. Lett. **29**(4), 398–399 (1993).
17. D. Chen and X. Cheng, "Hydrostatic pressure sensor based on a gold-coated fiber modal interferometer using lateral offset splicing of single mode fiber," Prog. Electromagnetics Res. **124**, 315–329 (2012).
18. W. Talataisong, D. N. Wang, R. Chitaree, C. R. Liao, and C. Wang, "Fiber in-line Mach-Zehnder interferometer based on an inner air-cavity for high-pressure sensing," Opt. Lett. **40**(7), 1220–1222 (2015).
19. C. M. Jewart, Q. Wang, J. Canning, D. Grobnic, S. J. Mihailov, and K. P. Chen, "Ultrafast femtosecond-laser-induced fiber Bragg gratings in air-hole microstructured fibers for high-temperature pressure sensing," Opt. Lett. **35**(9), 1443–1445 (2010).
20. R. M. Christensen, "Mechanics of cellular and other low-density materials," Int. J. Solids Struct. **37**(1-2), 93–104 (2000).
21. W. Primak and D. Post, "Photoelastic constants of vitreous silica and its elastic coefficient of refractive index," J. Appl. Phys. **30**(5), 779–788 (1959).
22. M. Xu, H. Geiger, and J. Dakin, "Fibre grating pressure sensor with enhanced sensitivity using a glass-bubble housing," Electron. Lett. **32**(2), 128–129 (1996).
23. A. Anuszkiewicz, G. Statkiewicz-Barabach, T. Borsukowski, J. Olszewski, T. Martynkien, W. Urbanczyk, P. Mergo, M. Makara, K. Poturaj, T. Geernaert, F. Berghmans, and H. Thienpont, "Sensing characteristics of the rocking filters in microstructured fibers optimized for hydrostatic pressure measurements," Opt. Express **20**(21), 23320–23330 (2012).
24. I. M. White and X. Fan, "On the performance quantification of resonant refractive index sensors," Opt. Express **16**(2), 1020–1028 (2008).
25. K. Nakajima, K. Hogari, J. Zhou, K. Tajima, and I. Sankawa, "Hole-assisted fiber design for small bending and splice losses," IEEE Photonics Technol. Lett. **15**(12), 1737–1739 (2003).